# Synthesis of hexagonal boron nitride 2D layers using polymer derived ceramics route and derivatives

Boitumelo Matsoso, Wenjun Hao, Yangdi Li, Victor Vuillet-A-Ciles, Vincent Garnier, Philippe Steyer, Bérangère Toury, Catherine Marichy, Catherine Journet

# Synthesis of hexagonal boron nitride 2D layers using polymer derived ceramics route and derivatives

**Boitumelo Matsoso[1], Wenjun Hao[1], Yangdi Li[1,2], Victor Vuillet-a-Ciles[1], Vincent Garnier[2], Philippe Steyer[2], Bérangère Toury[1], Catherine Marichy[1] and Catherine Journet[1*]**

[1] Laboratoire des Multimatériaux et Interfaces, UMR CNRS 5615, Univ Lyon, Université Claude Bernard Lyon 1, F-69622 Villeurbanne, France.
[2] Université de Lyon, MATEIS, UMR CNRS 5510, INSA-Lyon, F-69621 Villeurbanne cedex, France

E-mail: catherine.journet@univ-lyon1.fr

Received xxxxxx
Accepted for publication xxxxxx
Published xxxxxx

## Abstract

Hexagonal boron nitride (h-BN) is nowadays an increasingly attractive material, especially for two-dimensional material applications, due to its intrisic properties. However, its properties are highly dependent on the used synthesis approach. The Polymer Derived Ceramics (PDCs) route allows elaboration of h-BN with tailored textural and structural properties. Here, we demonstrate the interest of the PDCs pathway for the synthesis of h-BN. Growth of h-BN single crystals with crystal sizes of a few microns at relatively low temperature and atmospheric pressure is successfully achieved from borazine precursor using PDCs. The crystallization is improved by additivation of 5 wt% of $Li_3N$ to the pre-ceramic polymer. Furthermore, by coupling PDCs with gas pressure sintering, starting from the same pre-ceramic polymer and 25 wt% of $Li_3N$, the crystal size is enlarged up to hundreds of microns. The fabricated single crystals of pure h-BN can then be exfoliated into h-BN nanosheets. Finally, by combining PDCs with atomic layer deposition, functional BN nano-/hetero-structures are successfully synthesized from highly structured sensitive templates, making this ALD process a promising alternative for fabricating functional BN nanostructures.

Keywords: hexagonal boron nitride, polymer derived ceramics, atomic layer deposition, sintering, nanosheets, 2D material

## 1. Introduction

### *1.1 Hexagonal Boron Nitride (h-BN)*

Until its discovery as natural state in 2014,(1) boron nitride (BN) has only been known as a synthetic ceramic. It presents an elemental B/N ratio of 1. BN is isoelectronic of carbon with its constituents belonging to III and V groups. As carbon, BN displays a variety of structures, such as hexagonal (h-BN), cubic (c-BN), wurtzite (w-BN) and amorphous phases.(2) w-BN and c-BN are both $sp^3$ structures, the latter being the hardest material just after diamond, while h-BN evidences a $sp^2$ layered structure, in which the atomic planes are linked together by weak Van der Waals' interactions.(3) h-BN presents a low density (2.28)(4) and an electrical insulating behavior (indirect bandgap at

5.955 eV)(5) due to delocalized π-electrons on nitrogen atoms. Moreover, it displays a high thermal conductivity (up to 20 W/m.K)(6) allowing heat dissipation, strong high temperature stability (900-1000°C under air and up to 2800 °C under inert atmosphere) and a chemical inertness without toxicity making it an interesting environmental-friendly material. Finally, its lamellar structure brings it a solid lubricant behavior with a low friction coefficient (0.2-0.7).(7,8) The unique sum of all its properties makes h-BN a refractory ceramic, an additive powder in cosmetic, paints or dental cements and a lubricant in metallurgy.(2,9,10) At a lower scale, the extraordinary insulating and thermal-conducting properties of h-BN also ensures new applications in lightweight, high-performance mobile and flexible electronic systems.(11,12) With future applications in mind, it becomes urgent to develop miniaturized functional devices that can be used in relevant research fields, essentially in the electronic field.(4) For example, in its two-dimensional (2D) form, boron nitride is an excellent dielectric material that can be used as substrate for two-dimensional nanomaterials,(13,14) intercalant in Van der Waals heterostructures,(14,15) insulated gate dielectric(16) and counter electrode in dye-sensitized solar cells.(17) Thus, low dimensional h-BN have become among the most needed inorganic nanosystems.(18) Up to now, there are two main strategies to produce Boron Nitride NanoSheets (BNNSs), involving either a "bottom-up" or "top-down" approach.(19) Bottom-up routes mainly include Chemical Vapor Deposition (CVD),(20–24) whereas top-down ones rely on mechanical(19,25,26) or chemical(27) exfoliation from bulk h-BN crystals. Since many years, the Poymer Derived Ceramics (PDCs) route has been used for the synthesis of different kinds of boron nitride materials, from bulk to nanostructures.(28–31) Recently, it has demonstrated a high potential for the fabrication of bulk h-BN crystals that can be further exfoliated into BNNSs.(32–36)

### *1.2 Polymer Derived Ceramics (PDCs) route*

The PDCs has been first mentioned in the sixties by Chantrell and Popper (37) for the design and the synthesis of advanced non-oxide ceramics with a compositional and structural homogeneity.(29) One of the most appealing advantage is that, starting from molecular or preceramic polymeric precursors, specific shapes including ceramic fibers, films or composite materials, which cannot be easily obtained by conventional powder technology, can be produced. Preceramic polymers can indeed be processed or shaped using conventional polymer-forming techniques, and further converted into dense ceramics using thermal treatments.(31) Therefore, a number of precursors have been developed for the PDCs route in order to tune the shaping properties of the preceramic polymer. Concerning the synthesis of h-BN, borane-based and borazine-based compounds are mainly used. Their synthesis is reproducible and their ceramisation can be obtained with a high yield and high purity.

For many years, our lab works on synthesis of h-BN by the PDCs route giving rise to different shapes (fibers, coatings, foams, nanocages…).(38–43) More recently, our research efforts have been focused on the improvement of the PDCs route for h-BN nanomaterials fabrication. In this contribution, we will present results obtained with PDCs alone, PDCs combined with Gas Pressure Sintering (GPS) and with Atomic Layer Deposition (ALD).

## 2. Synthesis of hexagonal Boron Nitride nanomaterials using the PDCs route

### *2.1 Synthesis using PDCs alone*

Growth of large-area h-BN nanosheets at relatively low temperature and atmospheric pressure conditions is successfully achieved from borazine precursor using the PDCs route either without (h-$BN_0$) or with 5 wt.% (h-$BN_5$) $Li_3N$ added as crystallization agent to the pre-ceramic mixture. Ceramization is realized at 1400 °C under inert atmosphere to obtain BN material.

The morphology of the h-BN samples is investigated using Scanning Electron Microscopy (SEM). Figures 1a and b display typical SEM micrographs of the as-synthesized h-$BN_0$ and h-$BN_5$ samples, respectively. It can be observed that the h-$BN_0$ sample exhibits agglomerated and irregular grained nanocrystals comprising fractures and particles in jagged shapes and edges. On the other hand, the h-$BN_5$ sample reveals agglomerated, smooth-edged and well-defined platelike crystals with estimated diameter around 2 µm. Morphological properties of the h-BN samples is ascertained using Transmission Electron Microscopy (TEM). Low magnification TEM micrographs illustrate that addition of $Li_3N$ generates samples mainly composed of overlapping sheet-like structures, with crystal size less than 1 µm (Figure 1d), whereas growth without crystallization agent leads to the formation of an amorphous mass of undefined shape and dimensions (Figure 1c). Better crystallization in presence of $Li_3N$ is confirmed by both Raman spectroscopy and X-Ray Diffraction (XRD) data.

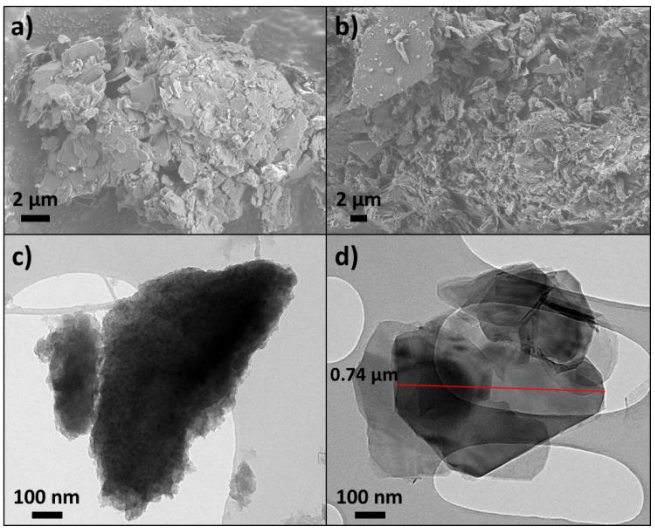


**Figure 1.** a-b) SEM and c-d) low magnification TEM micrographs of h-BN nanosheets grown from pure PBN (h-$BN_0$, a,c)) and PBN additivated with 5 wt% $Li_3N$ (h-$BN_5$, b, d)). The length of the sheet is pointed out by the red line.

Composition and crystallinity of the synthesized samples are examined by powder XRD (Figure 2a). Diffraction patterns, indexed using the JCPDS 00-034-0421 h-BN reference file, show formation of not well-crystallized h-$BN_0$ sample, as indicated by the very broad and undefined (002) and (100) peaks (Figure 2a (i)). On the other hand, the h-$BN_5$ diffractogram reveals the formation of two phases of boron nitride: hexagonal (h-BN) and rhombohedral (r-BN, JCPDS card n°00-045-1171) ones (Figure 2a (ii)). Furthermore, improved crystallinity of h-BN nanosheets is evidenced by symmetrical sharpening of the (002) peak, as well as the appearance of (004), (110), and (112) peaks. Addition of $Li_3N$ leads to reaction with PBN forming $Li_3BN_2$, which is known to dissolve BN.(44) Therefore, B-N nuclei would form and would agglomerate, grow and crystallize into BN domains. However, the preferential crystallization into h-BN or r-BN remains challenging.

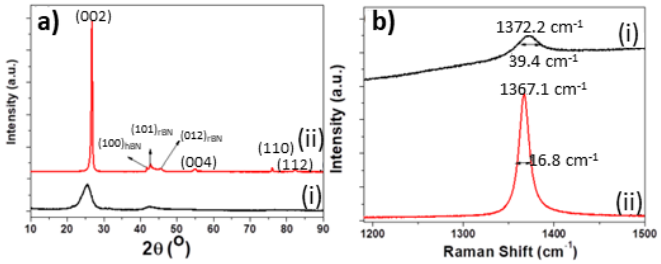


**Figure 2.** a) XRD patterns and b) Raman spectra of h-BN nanosheets grown (i) without and (ii) with addition of 5 wt% $Li_3N$. The peaks are indexed to the corresponding cristallographic planes in a) and the positions and FWHM of the h-BN $E_{2g}$ band are underlined in b).

The synthesized materials are investigated using Raman spectroscopy. Figure 2b displays average Raman spectra of ten different areas of the h-BN samples grown with (Figure 2b (ii)) and without (Figure 2b (i)) $Li_3N$. Spectra depict the presence of the first-order active Raman vibrating mode of h-BN ($E_{2g}$) at ~1367 $cm^{-1}$ and ~1372 $cm^{-1}$ for h-$BN_5$ and h-$BN_0$, respectively. The location, expected at 1366 $cm^{-1}$ for well-crystallized h-BN, and sharpening of the peak prove that addition of crystallization promoter permits improving the crystallinity of the BNNSs.(25,45,46) This is further confirmed by the value of the full width at half maximum (FWHM) of the $E_{2g}$ peak determined to be 16.8 $cm^{-1}$ and 39.4 $cm^{-1}$ for h-$BN_5$ and h-$BN_0$, respectively. Indeed, the lower is the FWHM value, the higher is the crystalline quality of the sample. Watanabe *et al.* report a FWHM of ~7 $cm^{-1}$ for high-purity h-BN single crystals. (25,45,46) Raman data are thus in good agreement with the obtained SEM, TEM and XRD results, indicating the influence of the addition of $Li_3N$ to the crystallinity of the BNNSs.

### *2.2 Synthesis using PDCs combined with Gas Pressure Sintering (GPS)*

As demonstrated, addition of a crystallization promoter allows improving the quality of the obtained h-BN. To synthesize large size high-quality h-BN crystals, the PDCs route is coupled with a sintering process, i.e. the Gas Pressure Sintering (GPS). From similar mixture of PBN and 25 wt% of $Li_3N$, after GPS process, shiny transparent material is collected either from the top inner surface or the bottom of the crucible (Figures 3c and 4c).

The transparent crystals located on the top inner surface of the crucible show very well defined hexagonal shapes up to dozens of microns, with smooth surfaces and sharp edges (Figure 3a,b). They are stacked in a layered 2D structure and show different orientations, which could be due to growth conditions. Actually, as mentioned in previous studies,(47) the reaction occuring between PBN and $Li_3N$ leads to an intermediate $Li_3BN_2$ compound at about 860 °C. At the melting temperature of $Li_3BN_2$ (920 °C), the compound would evaporate inside the crucible, and reach its top inner surface(47) that would act as nucleation seed allowing the BN crystallization. This implies that the crystallization occurs by nucleation from the vapor phase.

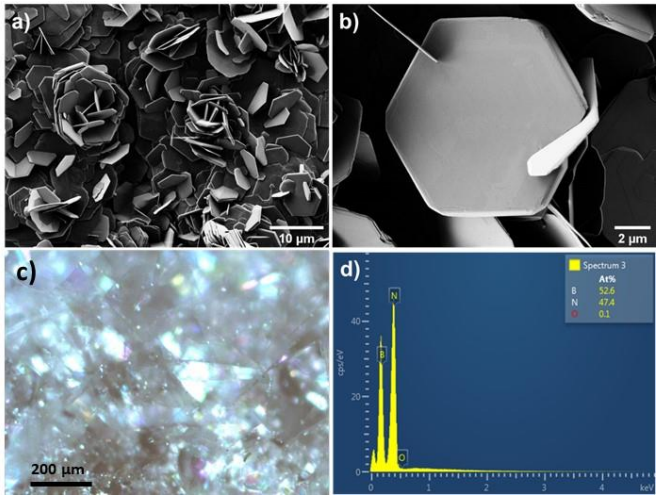


**Figure 3.** a,b) Low resolution SEM micrographs of the h-BN sample located on the top inner surface of the crucible. In a) faceted flower-like crystals are observed and b) shows the detail of one h-BN crystal. Corresponding c) optical image and d) EDS spectrum recorded using SEM.

Concerning the sample collected from the bottom of the crucible, SEM characterization shows different features with larger flakes up to hundreds of microns without hexagonal shape but still stacked into layered structure (Figure 4a, b). These characteristics are close to the ones previously observed for synthesis of h-BN combining PDCs route with spark plasma sintering process.(34) In that case, we can assume that the growth occurs in the liquid phase and the proposed crystallization mechanism would be similar to one of the previous studies reported by Bezrukov (48) and other groups.(47,49,50) At around 600–700 °C, $Li_3BN_2$ formed by reaction between $Li_3N$ and preceramic BN, melts and infiltrates amorphous BN and dissolves it, leading to highly crystallized hexagonal boron nitride.

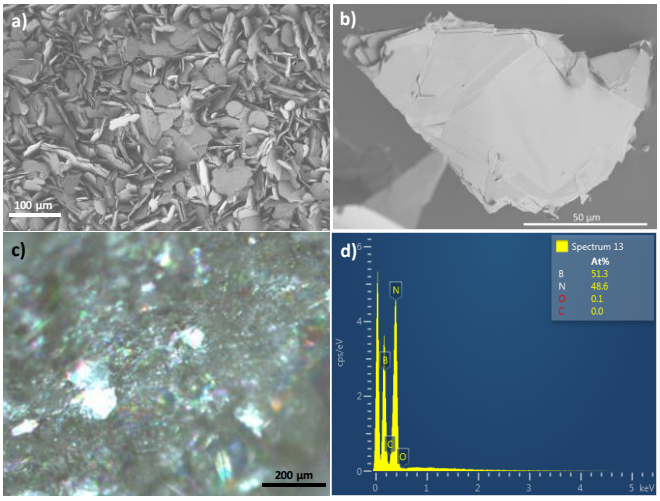


**Figure 4.** a,b) Low resolution SEM micrographs of the h-BN sample located on the bottom face of the crucible. In a) faceted crystals are observed and in b) one h-BN single flake with lateral size over 100 µm is shown. Corresponding c) optical image and d) EDS spectrum recorded using SEM.

Chemical analyses conducted by Energy Dispersion Spectroscopy (EDS) (Figures 3d and 4d) show an elemental composition of 52.6 at% B and 47.4 at% N (top inner part) and 51.3 at% B and 48.6 at% N (bottom part), confirming the synthesis of h-BN. The oxygen detected is only 0.1 at%, which is out of the EDS instrument sensitivity and accuracy.

Structural characterization by means of XRD and Raman spectroscopy shows exactly the same features whether it is on top and bottom parts. Figure 5a presents the XRD pattern of the sintered product. Compared with JCPDS 00-034-0421 file, all h-BN characteristic peaks can be assigned in the diffractogram, without any unexpected peaks. The diffraction pattern confirms the hexagonal structure with a lattice constant c of 6.66 Å. The integrated intensity ratio between (100) and (002) peak is about 0.21, which is slightly higher than the theoretical value of 0.15 for polycrystalline h-BN. This means that the sintering conditions promote growth along the c-axis.

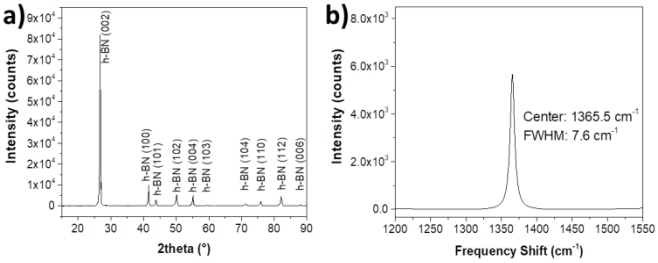


**Figure 5.** a) XRD pattern and b) Raman spectrum of h-BN samples obtained by PDCs coupled with GPS. The peaks are indexed to the corresponding cristallographic planes in a) and the position and FWHM of the h-BN $E_{2g}$ band are underlined in b).

Raman spectrum (Figure 5b), also displays very good signature of h-BN with well-defined single peak located at 1366 $cm^{-1}$, very close to the reference value of 1366.2 $cm^{-1}$.(51) This Raman peak, with a $E_{2g}$ symmetry, corresponds to the in-plane shearing mode of h-BN. One can notice that the measured FWHM value is only 7.6 $cm^{-1}$, close to that of the best quality h-BN single crystals fabricated by High Pressure High Temperature (HPHT) method (7.3 $cm^{-1}$).(52) This low FWHM value is a further proof of a highly crystallized h-BN structure.

In order to demonstrate the ability of these crystals to be used as BNNSs supply, exfoliation of nanosheets has been performed by ultra-sonication in ethanol medium. The obtained nanolayers have been then deposited on a TEM copper grid (300 mesh) covered with holey carbon. Figure 6 presents representative micrographs obtained on exfoliated h-BN. Low resolution TEM shows h-BN nanosheets (Figure

6a) as proven by Selected Area Electron Diffraction (SAED) (inset figure 6a) which clearly exhibits hexagonal bright dots, representative of single crystal. It is possible to determine the number of layers by counting the dark lines separated by interatomic distance (3.33 Å) on the edges of the sheet. Figure 6b confirms that they are very thin with an average number of layers around 3-4. The High Resolution Transmission Electron Microscopy (HRTEM) performed on a fine zone of one sheet shows the perfect atomic in-plane arrangement characteristic from the hexagonal lattice (Figure 6c).

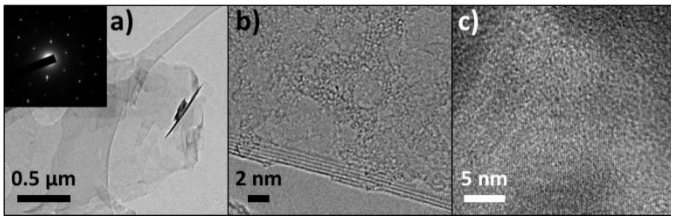


**Figure 6.** a) Low resolution TEM image of a h-BN nanosheet with in inset the corresponding SAED pattern showing the six diffraction spots of the hexagonal phase. b) edge of a h-BN nanosheet showing five stacked layers and c) high resolution TEM image recorded from a thin BN sheet where, due to interference with well cristalline material, alternating contrast (bright and dark dots) is observed.

In this part, we have demonstrated for the first time the synthesis of h-BN crystals by the unique combination of PDCs route and GPS method. The chemical and structural quality of the samples has been evidenced by use of EDS, XRD and Raman spectroscopy. This hybrid process allows synthesizing h-BN crystals with large lateral size (from tens to hundreds of microns) that can be used as BNNSs supply as proven by TEM.

### *2.3 PDCs route applied to Atomic Layer Deposition (ALD) of Boron Nitride*

PDCs and PDCs coupled with GPS are highly promising for production of self-standing h-BN single crystals that can be exfoliated into BNNSs. In order to widen the range of applications, it can be necessary to directly synthesize the BN nanosheets with a controlled number of layers. In this regards, ALD appears suitable. Indeed, it is a deposition technique producing highly reproducible, conformal and homogeneous thin films even on high aspect ratio substrates. Briefly, it is based on a reaction between precursor materials, separated into successive surface reactions. The reactants are kept separated and react with surface species in a self-limiting manner, i.e. without gas phase reaction. Each surface reaction is separated by a purge step to remove the unreacted precursor and the by-product. The succession of self-limited reactions and purges constitutes a cycle. The thickness of the deposit is simply determined by the number of cycles applied, allowing its control at the atomic level. ALD processes exist for a large variety of material classes, such as metals, oxides, nitrides, sulfides and phosphates.(53) Few processes have been developed for BN deposition. They are mainly based on use of ammonia and/or boron halide.(54) In 2018, a low temperature process based on electron enhanced ALD was reported. Even though this approach is promising for depositing crystalline BN on flat substrates, it is unsuitable for structured substrates.(55)

Offering a large panel of precursors and allowing pre-ceramic polymerization at low temperature, adaptation of the PDCs route to ALD appears as an elegant approach. Indeed, it permits developing a novel two-step ALD route that consists in: (1) deposition of a pre-ceramic polymer intermediate by ALD, (2) followed by its conversion into dense BN using a thermal annealing. Such two-step ALD approach has been previously reported for $MoS_2$. An amorphous organometallic intermediate is indeed deposited prior its conversion into crystalline 2D $MoS_2$ by thermal treatment.(56)

As precursors must fulfill several requirements such as thermal stability, sufficient vapor pressure and inertness towards themselves, trichloroborazine (TCB), a borazine derivative, reacted with hexamethylsilazane (HMDS) are chosen as ALD precursors. During the 1$^{st}$ ALD step, the pre-ceramic intermediate called polyborazine, $[B_3N_4H_4]_n$, is deposited at low temperature (80 °C) with a controlled thickness under release of trimethylsilyl chloride ($(CH_3)_3SiCl$). During the 2$^{nd}$ step, the formed amorphous polyborazine film is thermally converted into dense BN layers under release of $H_2$ and $NH_3$.

Due to the low temperature of the 1$^{st}$ step, various substrates, including polymer templates, are coated in a reproducible manner using the ALD route, demonstrating the versatility of the approach. Characteristic linear relationship between the thickness of the intermediate as well as of the final BN film and the number of cycles is reported, the growth per cycle (GPC) being 0.19 nm cycle$^{-1}$.(57) Uniform and conformal BN thin films or nanostructures, when templates are used, are successfully fabricated after thermal annealing under controlled atmosphere. XPS analysis reveals a close stoichiometry with a B/N ratio of 0.95 and no Cl contamination is noted.(57) Depending on the substrate, BN layers display either amorphous, turbostratic (t-BN) or hexagonal phase as visible in Figure 7. HRTEM image recorded from BN coated Si (100) wafer with native oxide after annealing at 1000 °C (Figure 7b) reveals the presence of very few lattice fringes indicating a near amorphous BN film on top of the Si wafer. Low magnification micrograph shows the formation of an amorphous interface of 13 nm between the Si substrate and the 45.6 nm thick BN layer. It can be attributed to the native $SiO_2$ layer and the potential

formation of a $B_xO_y/SiO_x$ mix layer (Figure 7a). On the other side, crystalline materials are observed after ALD on PC membrane (Figure 7c) and PAN fibers (Figure 7d) which both act as templates. Inverse structures are thus fabricated using ALD followed by annealing at 1400 °C partially under $NH_3$ to remove the soft template. Nanotube arrays and mats are respectively obtained with controlled thickness of the walls. Furthermore, carbon materials like amorphous carbon fibers are uniformly coated with polyborazine layer as nicely shown by Scanning Transmission Electron Microscopy (STEM) and EDS elemental mapping distribution (Figure 8a-d). The deposited pre-polymer layer leads then to either amorphous or t-BN (Figure 8e,f) film depending on the annealing temperature. Besides the influence of the heat treatment, difference in term of crystallinity is also noted as a function of the nature of the polymer support. Interaction between the organic support and the precursor as well as the creation of a polymer/inorganic interface can take place resulting in precursor infiltration into the polymeric chains(58,59) and higher GPC value is noted. In the present case, reactant infiltration impacts the structure of the final material. Indeed, according to the respective GPC value, i.e. 0.28 and 0.20 nm $cycle^{-1}$ on PAN and PC, and TEM characterization, no significant precursor diffusion seems to take place in case of ALD on PC and high crystalline BN material is fabricated (Figure 7c), whereas less-crystallized t-BN (Figure 7d) results from PAN template due to TCB precursor interaction with the soft template.

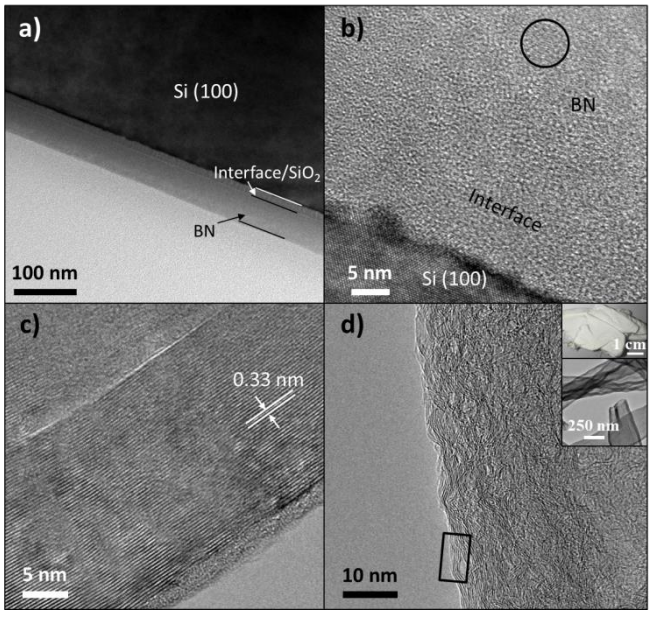


**Figure 7.** a, b) Cross-sectional TEM images at a) low and b) high resolution of BN coated Si (100) wafer with native oxide after annealing at 1000 °C. The black circle in b) points out the presence of very few lattice fringes. c, d) HRTEM micrographs of an external wall of BN nanotubes obtained from c) PC membrane(57) and d) PAN fibers. Well-defined lattice fringes with an atomic inter-distance of 0.33 nm are visible in both cases, as evidenced by the black square in d). In inset d), the corresponding micrograph (top) and the TEM image (bottom) of unwoven BN nanotube mat.

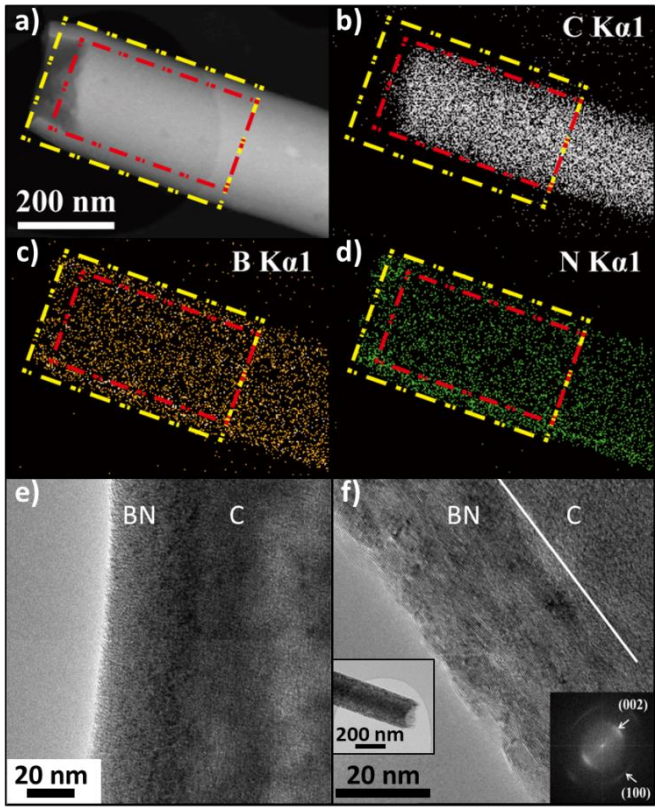


**Figure 8.** a) STEM micrograph and b,c,d) the corresponding C, B and N elemental EDS mapping distribution of a polyborazine coated carbon fiber. e and f) HRTEM micrographs of BN coated carbon fibers after annealing at, respectively, e) 1000 °C and f) 1400 °C under Ar. Insets in f): TEM image of the fiber (left) and the corresponding calculated diffraction pattern (right) exhibiting the two main d-spacing of the hexagonal BN phase.

Enabling use of highly structured sensitive templates, our ALD approach is successful for synthesizing functional BN nano-/hetero-structures. In particular, the fabricated BN nanostructures show great potential in water treatment. While only weak hydrophilicity and high lipophilicity are displayed by BN films on $SiO_2$/Si surface, unwoven BN nanotube mats exhibit super-hydrophobicity as well as good lipophilicity and good stability towards aging under air and drastic pH conditions. They demonstrate efficient as filter to separate water from organic solvents and excellent performances for organic absorption with reusable properties.(60) Moreover, BN films reveal suited as protective coating. BN coated carbon nanotubes exhibit improved oxidation resistance by near 100 °C compared to the uncoated carbon material as demonstrated by thermogravimetric analysis (TGA) (Figure 9).(61)

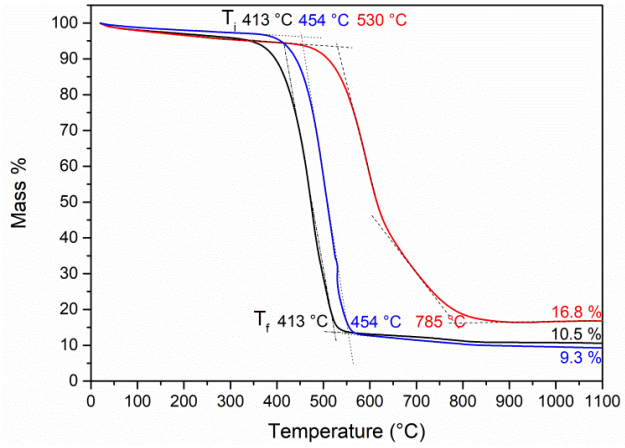


**Figure 9.** TGA curves of bare carbon nanotubes (black curve), carbon nanotubes after annealing at 1400 °C under Ar (blue curve) and BN ALD coated carbon nanotubes after annealing at 1400 °C under Ar (red curve). $T_i$: decomposition onset temperature and $T_f$: offset temperature. The mass residue is indicated in percentage.

To conclude, two-step ALD process of BN based on polymer derived ceramics chemistry has been successfully reported. The process is versatile and represents a promising alternative to the existing processes. Despite the high temperature second step, the two-step ALD approach based on PDCs chemistry appears promising for fabricating h-BN nanostructures with controlled thickness. Indeed, the ALD step occurring at low temperature (80 °C) widen the range of substrates and paves the way to fabrication of functional BN nanostructures that require highly structured polymer template.

## 3. Conclusion

PDCs route has proven to be an effective route for synthesizing high quality h-BN materials. In particular, addition of a crystallization promoter, like $Li_3N$, allows good crystallinity at reduced temperature and atmospheric pressure. Moreover, use of GPS permits to enlarge the lateral size of BNNS up to hundreds of µm, while maintaining the crystal quality. Finally, ALD process based on PDCs route demonstrates to be an interesting approach for fabricating thin BN pre-ceramic films on various substrates that leads to well-defined BN nano-/hetero-structures.

These synthesized high quality boron nitride nanomaterials can find applications in various areas as micro-electronics, photonics and environmental domains. To conclude, the PDCs pathway is a versatile and efficient chemical method that can be combined with other techniques allowing tuning the shape and properties of the BN material.

## Methods

*Synthesis using PDCs alone*

Borazine is prepared from a reaction between ammonium sulphate ($(NH_4)_2SO_4$, ≥ 99 %, Aldrich) and sodium borohydride ($NaBH_4$, 98 % purity, Aldrich) in tetraethylene glycol dimethyl ether or tetraglyme ($C_{10}H_{22}O_5$, ≥ 99 %, Alfa Aesar) solvent, as reported by Wideman *et al.* (62). After the purification of borazine via distillation, a colourless pre-ceramic polymer, the PBN is obtained through the poly-condensation of borazine at 55 °C inside a pressure-sealed system under argon for 5 days.(29,38,39) Inside a glove box under argon atmosphere, lithium nitride ($Li_3N$, 99.4 %, Alfa Aesar), at a 5 wt% ratio, is added to PBN, as a crystallization agent. The mixture is homogenized via stirring for 10 min, after which the suspension is heated to 200 °C in an alumina crucible and kept for 1h to give a solid-state polymer.(32,33,63) Finally, the stabilized mixture is annealed for 1 h at 1400 °C (1 °C.min$^{-1}$) under inert nitrogen ($N_2$, 98 %, Air Liquide, France) atmosphere. As a control experiment, a similar procedure is followed using a pre-ceramic mixture comprised of PBN only. Finally, after cooling the furnace to room temperature, the h-BN samples are collected and labelled as h-$BN_5$ and h-$BN_0$, for samples prepared with 5wt.% of $Li_3N$ and without, respectively.

*Synthesis using PDCs combined with GPS*

The synthesis of PBN is made following the procedure described above. Then 25 wt% lithium nitride ($Li_3N$, 99.5 %, Aldrich) micro powder is dispersed as crystallization promoter into pure homemade liquid PBN. The dispersion is slowly heated in a glove box filled with argon from room temperature to 200 °C, and hold at this temperature for 1 h leading to a solid-state polymer avoiding further oligomer evaporation. The resulting solid is placed into an alumina crucible to be heated under $N_2$ to 650 °C (3 °C.min$^{-1}$), and kept at this temperature for 1 h. After heat treatment, the mixture is grinded into powder in the glove box.

For GPS experiment, the preceramic powder is firstly filled and enclosed in a pure BN crucible (5 mm internal diameter and 5 mm height) in a glove box and transferred into the GPS chamber. Before sintering, the chamber is vacuumed twice to remove the air residue. When starting the experiment, the chamber is filled with Ar and pressure is increased up to 95 bar. While keeping the pressure constant, the temperature ramps up to 2000 °C in 3 h. The furnace maintains this temperature for a 3-5 h dwelling. The pressure is kept until the end of dwelling.

*PDCs route applied to ALD of BN*

Depositions take place in a home-made ALD working in exposure mode. 2,4,6-tri(chloro)borazine (laboratory from ref (57)) and hexamethyldisilazane (ROTH, 98 %) are used as reactants. Their canisters are, respectively, kept at 70 and 30 °C. Deposition occurs at 80 °C with an opening time of 1 s and 0.05 s for TCB and HMDS, respectively. Each pulse is

followed by a residence and purge time of 10 s. Pure nitrogen is used as carrier gas at a constant flow rate of 5 sccm. Films are deposited on Si(100) wafer with native oxide. Millipore polycarbonate membranes, electrospun polyacrylonitrile fibers and carbon fibers (synthesized at the laboratory) are also coated using a simple home-made ALD reactor made of glassware.(57) All as-deposited thin films are post-annealed in a tubular furnace under inert atmosphere, and for polymer support partially under $NH_3$. All transfers are performed under controlled atmosphere to avoid exposure to air before annealing.

*Characterization techniques*

The synthesized BN materials are characterized by optical microscopy using a Zeiss Axiophot Photomicroscope as well as by SEM using a FEG-SUPRA Zeiss 55VP microscope operating at 800V with an Oxford X-Max Silicon Drift EDS detector and a Zeiss Merlin VP compact microscope operated at 5 kV and equipped with a SDD OXFORD X-Max EDS detector. Samples were prepared without carbon or platinum coating. TEM, HRTEM and high-angle annular dark-field STEM investigations are carried out on 300 mesh copper TEM grids covered with a holey carbon support film using a JEOL 2100F and JEOL 2010F microscopes both operated at 200 kV and equipped with silicon drift detector (Oxford Instrument) for EDS. Cross-section of boron nitride thin film on Si substrate is realized using mechanical polishing followed by ion etching using Precision Ion Polishing System (PIPS) 691 from Gatan. In addition to TEM studies, the crystalline quality of the BN materials is characterized by powder XRD and Raman spectroscopy. XRD is carried out with a Bruker D8 Advance diffractometer, using CuK radiation source, $\lambda = 1.5418$ Å, and the Raman spectra are recorded using a Labram HR800 spectrometer (HORIBA Jobin-Yvon) with 532 nm laser excitation wavelength. XPS is performed, using a PHI Quantera SXM spectrometer with Al Kα monochromatism radiation, to characterize the composition of the deposited material. Sample is kept on the holder using carbon paste. The raw XPS data are corrected using the binding energy of the C-C bond at 284.5 eV and fitted with Gaussian-Lorentzian curves. Finally, the thickness of the deposited ALD BN films on the wafer substrates are measured by ellipsometry spectroscopy at an incidence angle of 70° using a Sopra GES-5E spectrometer. Data fit is realized with the "Winell II" software using Cauchy dispersion law. The protective property towards oxidation of the BN coating is evaluated by thermogravimetric analysis using a TGA/DSC2 Mettler Toledo thermobalance with a temperature ramp of 10 °C.min$^{-1}$ until 1100 °C under air.

## Acknowledgements

The authors thank the "Centre Technologique des Microstructures", CTμ, (Université Lyon 1), the CLYM, for providing access to the TEM and SEM facilities, CECOMO for access to Raman spectroscopy and Science et Surface (Ecully, France) for XPS analyses. V. Salles and D. Fournier are kindly acknowledged for the electrospun PAN fibers and TGA analyses, respectively.

This work has been partially financially supported by the European Union Horizon 2020 Program under the Graphene Flagship (grant number 785219), the iMUST LABEX program MUSCAT-2D and the National Research Agency, France (project n° ANR-16-CE08-0021-01). W. Hao and Y. Li acknowledge the China Scholarship Council (CSC) for the PhD grant support.

## References

1. Dobrzhinetskaya LF, Wirth R, Yang J, Green HW, Hutcheon ID, Weber PK, et al. Qingsongite, natural cubic boron nitride: The first boron mineral from the Earth's mantle. American Mineralogist. 2014;99(4):764–72.

2. Haubner R, Wilhelm M, Weissenbacher R, Lux B. Boron Nitrides — Properties, Synthesis and Applications. In: Jansen M, editor. High Performance Non-Oxide Ceramics II. Berlin, Heidelberg: Springer Berlin Heidelberg; 2002. p. 1–45.

3. Constantinescu G, Kuc A, Heine T. Stacking in Bulk and Bilayer Hexagonal Boron Nitride. Physical Review Letters. 2013;111(3).

4. Wang J, Ma F, Liang W, Sun M. Electrical properties and applications of graphene, hexagonal boron nitride (h-BN), and graphene/h-BN heterostructures. Materials Today Physics. 2017;2:6–34.

5. Cassabois G, Valvin P, Gil B. Hexagonal boron nitride is an indirect bandgap semiconductor. Nature Photonics. 2016;10(4):262–6.

6. Zheng J-C, Zhang L, Kretinin AV, Morozov SV, Wang YB, Wang T, et al. High thermal conductivity of hexagonal boron nitride laminates. 2D Mater. 2016;3(1):011004.

7. Rowe GW. Some observations on the frictional behaviour of boron nitride and of graphite. Wear. 1960;3(4):274–85.

8. Martin JM, Mogne TL, Chassagnette C, Gardos MN. Friction of Hexagonal Boron Nitride in Various Environments. Tribology Transactions. 1992;35(3):462–72.

9. Engler M, Lesniak C, Damasch R, Ruisinger B, Eichler J. Hexagonal Boron Nitride (hBN) – Applications from Metallurgy to Cosmetics. Ceramic Forum International. 2007;84:E49-53.

10. Lipp A, Schwetz KA, Hunold K. Hexagonal boron nitride: Fabrication, properties and applications. Journal of the European Ceramic Society. 1989;5(1):3–9.

11. Akinwande D, Petrone N, Hone J. Two-dimensional flexible nanoelectronics. Nature Communications. 2014;5:5678.

12. Cai Z, Liu B, Zou X, Cheng H-M. Chemical Vapor Deposition Growth and Applications of Two-Dimensional Materials and Their Heterostructures. Chemical Reviews. 2018;118(13):6091–133.

13. Kim KK, Hsu A, Jia X, Kim SM, Shi Y, Dresselhaus M, et al. Synthesis and Characterization of Hexagonal Boron Nitride Film as a Dielectric Layer for Graphene Devices. ACS Nano. 2012;6(10):8583–90.

14. Dean CR, Young AF, Meric I, Lee C, Wang L, Sorgenfrei S, et al. Boron nitride substrates for high-quality graphene electronics. Nat Nano. 2010;5(10):722–6.

15. Geim AK, Grigorieva IV. Van der Waals heterostructures. Nature. 2013;499(7459):419–25.

16. Britnell L, Gorbachev RV, Jalil R, Belle BD, Schedin F, Katsnelson MI, et al. Electron Tunneling through Ultrathin Boron Nitride Crystalline Barriers. Nano Letters. 2012;12(3):1707–10.

17. Xu SJ, Luo YF, Zhong W, Xiao ZH, Liu XY. Investigation of Hexagonal Boron Nitride for Application as Counter Electrode in Dye-Sensitized Solar Cells. Advanced Materials Research. 2012;512–515:242–5.

18. Wang J, Ma F, Sun M. Graphene, hexagonal boron nitride, and their heterostructures: properties and applications. RSC Adv. 2017;7(27):16801–22.

19. Zhang K, Feng Y, Wang F, Yang Z, Wang J. Two dimensional hexagonal boron nitride (2D-hBN): synthesis, properties and applications. J Mater Chem C. 2017;5(46):11992–2022.

20. Khan MH, Liu HK, Sun X, Yamauchi Y, Bando Y, Golberg D, et al. Few-atomic-layered hexagonal boron nitride: CVD growth, characterization, and applications. Materials Today. 2017;20(10):611–28.

21. Lee JS, Choi SH, Yun SJ, Kim YI, Boandoh S, Park J-H, et al. Wafer-scale single-crystal hexagonal boron nitride film via self-collimated grain formation. Science. 2018;362(6416):817–21.

22. Lu G, Wu T, Yuan Q, Wang H, Wang H, Ding F, et al. Synthesis of large single-crystal hexagonal boron nitride grains on Cu–Ni alloy. Nat Commun. 2015;6(1):1–7.

23. Gibb AL, Alem N, Chen J-H, Erickson KJ, Ciston J, Gautam A, et al. Atomic Resolution Imaging of Grain Boundary Defects in Monolayer Chemical Vapor Deposition-Grown Hexagonal Boron Nitride. Journal of the American Chemical Society. 2013;135(18):6758–61.

24. Ismach A, Chou H, Ferrer DA, Wu Y, McDonnell S, Floresca HC, et al. Toward the Controlled Synthesis of Hexagonal Boron Nitride Films. ACS Nano. 2012;6(7):6378–85.

25. Gorbachev RV, Riaz I, Nair RR, Jalil R, Britnell L, Belle BD, et al. Hunting for Monolayer Boron Nitride: Optical and Raman Signatures. Small. 2011;7(4):465–8.

26. Novoselov KS, Jiang D, Schedin F, Booth TJ, Khotkevich VV, Morozov SV, et al. Two-dimensional atomic crystals. Proceedings of the National Academy of Sciences of the United States of America. 2005;102(30):10451–10453.

27. Coleman JN, Lotya M, O'Neill A, Bergin SD, King PJ, Khan U, et al. Two-Dimensional Nanosheets Produced by Liquid Exfoliation of Layered Materials. Science. 2011;331(6017):568–71.

28. Paciorek KJL, Masuda SR, Kratzer RH, Schmidt WR. Processible precursor for boron nitride coatings and matrixes. Chem Mater. 1991;3(1):88–91.

29. Bernard S, Miele P. Polymer-derived boron nitride: A review on the chemistry, shaping and ceramic conversion of borazine derivatives. Materials. 2014;7(11):7436–59.

30. Paine RT, Narula CK. Synthetic routes to boron nitride. Chem Rev. 1990;90(1):73–91.

31. Colombo P, Mera G, Riedel R, Sorarù GD. Polymer-Derived Ceramics: 40 Years of Research and Innovation in Advanced Ceramics: Polymer-Derived Ceramics. Journal of the American Ceramic Society. 2010;93(7):1805–37.

32. Yuan S, Toury B, Journet C, Brioude A. Synthesis of hexagonal boron nitride graphene-like few layers. Nanoscale. 2014;6(14):7838–41.

33. Yuan S, Toury B, Benayoun S, Chiriac R, Gombault F, Journet C, et al. Low-Temperature Synthesis of Highly Crystallized Hexagonal Boron Nitride Sheets with Li3N as Additive Agent. European Journal of Inorganic Chemistry. 2014;2014(32):5507–13.

34. Yuan S, Linas S, Journet C, Steyer P, Garnier V, Bonnefont G, et al. Pure & crystallized 2D Boron Nitride sheets synthesized via a novel process coupling both PDCs and SPS methods. Scientific Reports. 2016;6:20388.

35. Yuan S, Journet C, Linas S, Garnier V, Steyer P, Benayoun S, et al. How to Increase the h-BN Crystallinity of Microfilms and Self-Standing Nanosheets: A Review of the Different Strategies Using the PDCs Route. Crystals. 2016;6(5):55.

36. Li Y, Garnier V, Journet C, Barjon J, Loiseau A, Stenger I, et al. Advanced synthesis of highly crystallized hexagonal boron nitride by coupling polymer-derived ceramics and spark plasma sintering processes—influence of the crystallization promoter and sintering temperature. Nanotechnology. 2018;30(3):035604.

37. Chantrell PG, Popper P. Inorganic polymers for ceramics. Academic Press. New York: Popper; 1965. (Special Ceramics; vol. 4).

38. Cornu D, Miele P, Toury B, Bonnetot B, Mongeot H, Bouix J. Boron nitride matrices and coatings from boryl borazine molecular precursors. Journal of Materials Chemistry. 1999;9(10):2605–10.

39. Termoss H, Toury B, Brioude A, Dazord J, Le Brusq J, Miele P. High purity boron nitride thin films prepared by the PDCs route. Surface and Coatings Technology. 2007;201(18):7822–8.

40. Toury B, Miele P. A new polyborazine-based route to boron nitride fibres. J Mater Chem. 2004;14(17):2609–11.

41. Alauzun JG, Ungureanu S, Brun N, Bernard S, Miele P, Backov R, et al. Novel monolith-type boron nitride hierarchical foams obtained through integrative chemistry. J Mater Chem. 2011;21(36):14025–30.

42. Salles V, Bernard S. A Review on the Preparation of Borazine-Derived Boron Nitride Nanoparticles and Nanopolyhedrons by Spray-Pyrolysis and Annealing Process. Nanomaterials and Nanotechnology. 2016;6:1.

43. Salles V, Bernard S, Li J, Brioude A, Chehaidi S, Foucaud S, et al. Design of Highly Dense Boron Nitride by the Combination of Spray-Pyrolysis of Borazine and Additive-Free Sintering of Derived Ultrafine Powders. Chem Mater. 2009;21(13):2920–9.

44. Zhang X, Meng J. Chapter 4 - Recent progress of boron nitrides. In: Liao M, Shen B, Wang Z, editors. Ultra-Wide Bandgap Semiconductor Materials. Elsevier; 2019. p. 347–419. (Materials Today).

45. Stenger I, Schué L, Boukhicha M, Berini B, Plaçais B, Loiseau A, et al. Low frequency Raman spectroscopy of few-atomic-layer thick hBN crystals. 2D Mater. 2017;4(3):031003.

46. Kuzuba T, Era K, Ishii T, Sato T. A low frequency Raman-active vibration of hexagonal boron nitride. Solid State Communications. 1978 Mar 1;25(11):863–5.

47. Yamane H, Kikkawa S, Koizumi M. High-and low-temperature phases of lithium boron nitride, Li 3 BN 2: Preparation, phase relation, crystal structure, and ionic conductivity. Journal of Solid State Chemistry. 1987;71(1):1–11.

48. Bezrukov G, Butuzov V, Nikitina T, Feldgun L, Filonenk N, Khatelis G. On crystallization of cubic boron nitride and of synthetic diamond. Doklady Akademii Nauk Sssr. 1968;179(6):1326-.

49. Li S, Guo X, Xu B, Wang H. Fracture morphology and XRD layered characterization of cBN cake. J Synth Cryst. 2012;41:15–19.

50. Xu B, Lv M-Z, Yang H-M, Wen Z-X. Thermodynamic Analysis of the V-Shaped Area of High Pressure and High Temperature in Cubic Boron Nitride Synthesis with Li3N as a Catalyst. Entropy. 2014;16(2):912–920.

51. Nemanich RJ, Solin SA, Martin RM. Light scattering study of boron nitride microcrystals. Phys Rev B. 1981;23(12):6348–56.

52. Schué L, Stenger I, Fossard F, Loiseau A, Barjon J. Characterization methods dedicated to nanometer-thick hBN layers. 2D Mater. 2016;4(1):015028.

53. George SM. Atomic Layer Deposition: An Overview. Chem Rev. 2010;110(1):111–31.

54. Hao W, Marichy C, Journet C. Atomic layer deposition of stable 2D materials. 2D Mater. 2018;6(1):012001.

55. Sprenger JK, Sun H, Cavanagh AS, Roshko A, Blanchard PT, George SM. Electron-Enhanced Atomic Layer Deposition of Boron Nitride Thin Films at Room Temperature and 100 °C. J Phys Chem C. 2018;122(17):9455–64.

56. Cadot S, Renault O, Frégnaux M, Rouchon D, Nolot E, Szeto K, et al. A novel 2-step ALD route to ultra-thin MoS2 films on SiO2 through a surface organometallic intermediate. Nanoscale. 2017;9(2):538–46.

57. Hao W, Marichy C, Journet C, Brioude A. A Novel Two-Step Ammonia-Free Atomic Layer Deposition Approach for Boron Nitride. ChemNanoMat. 2017;3(9):656–63.

58. Parsons GN. Atomic Layer Deposition on Soft Materials. In: Atomic Layer Deposition of Nanostructured Materials. John Wiley & Sons, Ltd; 2012. p. 271–300.

59. Azpitarte I, Knez M. Vapor phase infiltration: from a bioinspired process to technologic application, a prospective review. MRS Communications. 2018;8(3):727–41.

60. Hao W, Marichy C, Brioude A. Promising properties of ALD boron nitride nanotube mats for water purification. Environ Sci: Nano. 2017;4(12):2311–20.

61. Hao W. Atomic layer deposition of boron nitride [phdthesis]. Université de Lyon; 2017.

62. Wideman T, Sneddon LG. Convenient Procedures for the Laboratory Preparation of Borazine. Inorganic Chemistry. 1995;34(4):1002–3.

63. Guo XF, Xu B, Zhang W, Lv MZ, Yang HM, Fan XH. Thermodynamic analysis about nucleation and growth of cubic boron nitride crystals in the hBN-Li3N system under high pressure and high temperature. Entropy. 2015;17(2):755–62.